Ocean Engineering 272 (2023) 113663

Contents lists available at ScienceDirect

Ocean Engineering

journal homepage: www.elsevier.com/locate/oceaneng

Pitching foil propulsion performance decays near the free surface

Francisco J. Huera-Huarte

Department of Mechanical Engineering, Universitat Rovira i Virgili (URV), 43007 Tarragona, Spain

ARTICLE INFO

Keywords:
Bio-inspired propulsion
Pitching foils
Swimming
Vortex wakes
Free surface

ABSTRACT

A series of experiments reveal the non-linear relationship between the propulsive performance of a pitching foil and its distance to the free surface. An especially designed robotic device allowed to sinusoidally actuate a symmetric NACA 0021 profile, with its shaft being perpendicular to the free surface, at different separations from it, whilst measuring hydrodynamic loads, power and efficiency. Digital Particle Image Velocimetry (DPIV) was used to study the flow structures around the flapping system, to better understand the performance trends observed.

Efficiency dropped more than a 40% when the foil was placed at a distance of approximately 5 to 10% of the span of the system, as a consequence of a large decrease in thrust and a large increase in power, both clearly linked to wake formation.

1. Introduction

Since the early studies of Lighthill (1960, 1969, 1970, 1971) a large amount of work has been published with the objective to understand fish locomotion because of its implications in biological, physical sciences and engineering. In the last decades, the use of simplified robotic systems or advanced simulations to emulate specific aspects of the locomotion of fish, has become widespread. By reproducing certain aspects of the swimming kinematics of fish, one can study in detail phenomena that would be very difficult to analyse with living fish. Earliest experiments in this direction by Triantafyllou et al. (1991, 1993) were used to study the mechanics of thrust production and wake formation with oscillating foils. Since then, hundreds of theoretical, numerical and experimental works have been published in the literature, covering a wide variety of aspects related to the analysis of the swimming of fish and bio-inspired systems. The reader is referred to some of the multiple existing reviews of the topic published in the last two decades (Sfakiotakis et al., 1999; Triantafyllou et al., 2000; Colgate and Lynch, 2004; Triantafyllou et al., 2005; Wu, 2011; Smits, 2019; Buren et al., 2020).

The case of fish swimming near boundaries is one of the many aspects to consider when thinking in fish locomotion. Benthic fish live and feed near the ground in the ocean and other water bodies, and a common guess was that some of these fish, could take advantage of swimming near the ground for increased efficiency and for the reduction of the cost of transport. The physics of ground effect associated to engineering applications such as in aircraft (Staufenbiel and Schlichting, 1988) and vehicles (Katz and Plotkin, 2001; Katz, 2006), are all based on fixed bodies and have been widely studied in the past. The case of fish or bio-inspired propulsion in ground effect has received less attention, although recent experiments (Quinn et al., 2014a,b; Fernández-Prats et al., 2015) have shown efficiency benefits for propulsion near a boundary. These works were inspired by the swimming of planniform species that live near the seabed. The kinematics imposed to their respective systems resulted from the sinusoidal actuation of a flexible foil using a shaft parallel to the ground. They found that the ground had a positive effect on the thrust generated due to enhanced circulation and the constrainment of momentum along the desired thrust direction.

Other fish move near the free surface for mating, feeding, escaping, etc. There are other not as obvious reasons for fish to swim near the free surface, for example, whale sharks need to thermo-regulate by swimming at the free surface, after long dives (Thums et al., 2013). In any case, future underwater vehicles based on biomimetic foils and bio-inspired robots will need to be designed for all sorts of situations, including propelling themselves near boundaries and therefore, these studies are of extreme relevance for ocean engineering systems.

The most common configuration when studying ground effect in fish like propulsion, is by orienting the actuating shaft of the system, parallel to the boundary. Cleaver et al. (2013) conducted experiments to study the effects of depth and amplitude on a NACA 0012 foil with forward motion by plunging an airfoil and imposing vertical heaving motion in a water tunnel. The authors compared the forces measured against those resulting from steady flow over the foil. It was found that proximity to the free surface increased drag and the surface waves altered the flow field near the foil minimizing thrust. Interestingly,

E-mail address: francisco.huera@urv.cat.

https://doi.org/10.1016/j.oceaneng.2023.113663
Received 4 October 2022; Received in revised form 4 January 2023; Accepted 7 January 2023
Available online 14 February 2023

there are not many works where the effect of the free surface is taken into account in a configuration in which the actuating shaft of the appendage that simulates the fin, is perpendicular to the free surface. Zhu et al. (2006) described computational results of a moving NACA 0012 foil of aspect ratios 1 and 5, with forward motion operating near the free surface in horizontal and vertical configurations. They found that the influence of the free surface was less important in the vertical configuration, because of a large part of the foil was deeply submerged, even for relatively small distances to the free surface. This is specially true for large aspect ratio foils. Barannyk et al. (2012) studied experimentally the performance of a heaving and pitching plate with blunt leading and trailing edges in a free-stream, with varying chord-wise flexibility and different submergence depths. They mention there is a clear non-linear effect of the boundaries on the propulsive performance of the system and that there is an evident increase in trust and efficiency, when the foil was moving near the solid boundary. They reported that this was not the case when approaching the free surface.

This paper studies the effect of proximity to the free surface on the performance of a vertical pitching foil. Hydrodynamic forces and efficiency have been measured and are presented together with Digital Particle Image Velocimetry (DPIV) measurements in the wake of the system, in Section 3. In Section 2, details about the experimental methods are given. To the knowledge of the author, there are no experimental results available in the literature, that report both types of measurements for this problem.

2. Experimental methods

The pitching foil used for the experiments was based on a NACA 0021 profile, with a chord c of 85 mm and a span s of 150 mm, 3D printed in PolyLactic Acid (PLA). The foil was attached to a 6 mm stainless steel shaft actuated by a servomotor, able to deliver 0.59 Nm at 6 V. A torque sensor, with a measurement range of ±5 Nm and an accuracy of ±0.2% of its full scale range, was installed between the servomotor and the foil allowing the measurement of the torque produced when the system was actuated. A rotary precision potentiometer (300 deg range with an accuracy of a 2%) was geared to the shaft near the servomotor to measure the imposed kinematics to the foil. An in-house developed code uploaded to dedicated electronics, allowed the control of the servo, powered by a laboratory power supply, using a Pulse Width Modulated (PWM) signal. The control system was designed to actuate sinusoidally the foil by setting the angular amplitude (θ_0) and the pitching frequency ($f = \omega/2\pi$), producing motions described by $\theta(t) = \theta_0 \sin(\omega t)$.

The robotic system was installed vertically, on top of the water tank of the Laboratory for Fluid-Structure Interaction at Universitat Rovira i Virgili, with a translucid working section of dimensions 1 × 1.1 × 2.25 m. It was installed hanging from a 6 axis load cell with a measurement range of 100 N for forces and 10 Nm for moments with accuracies that are 0.35% or better in all channels. The load cell was attached to an air bearing carriage guided by a rectangular beam with cross-section 50.8 × 50.8 mm^2 and a local straightness accuracy of 25 μm/m over its entire length. This arrangement ensured there was no friction between the carriage and the beam. The motion along the beam was restricted by a uni-axial precision load cell with a measurement range of ±8.9 N and an accuracy of 0.05% of its full scale range. This sensor was connected to the air bearing carriage and to an external fixed structure by means of universal joints, preventing the appearance of reaction moments on it. Hence, using this set-up, thrust force measurements were available redundantly, from the 6-axis and the uni-axial load cells. Both signals showed extremely good agreement with differences under 3%.

A Cartesian coordinate system is considered having its origin at the mid span point of the profile, with z along the main shaft and x aligned to the direction of the thrust force, imposed by the air bearing rig. The mechanical design allowed to adjust the distance (h) from the upper edge of the foil to the free surface. In order to study the effects of the proximity to the free surface, h was varied from 0 (upper edge at the free surface) to more than $1s$, condition at which results were observed not to be dependent on h. Experiments were conducted without a free stream, in quiescent fluid. This was made to avoid the formation of leading edge vortices and the undesired interactions of those with the trailing edge ones, that would yield complexity to the problem, not wanted at this stage. The signals output by all the sensors, including the shaft rotation, the torque, and the output of the multi-axis and the uni-axial load cells, were synchronously sampled at 2 kHz using a dedicated data acquisition system controlled by an in-house code developed for the experiments.

Time-Resolved Digital Particle Image Velocimetry (DPIV) was used to investigate the flow structures generated by the motion of the foil. Images were acquired at 500 fps using a CCD-sensor with 12 bit resolution, a pixel size of 10 μm and 1280 × 1024 pixels. The camera was fitted with a 20 mm fixed focal length objective and seeding was done, using 20 μm neutrally buoyant Polyamide particles. The illumination was provided by a continuous wave (CW) Diode-Pumped solid State (DPSS) green laser. Interrogations were done in two different planes, one cutting the foil at its mid span (xy) and another near the trailing edge, parallel to the rotating shaft at a distance slightly greater than the chord (yz). Image pre-processing using in-house codes was performed in order to mask regions without particles in the flow and to identify in each DPIV snapshot the position of the trailing edge. After this initial pre-processing, a Fast Fourier Transform (FFT) cross-correlation algorithm (Willert and Gharib, 1991) was applied to the pre-processed images, using an interrogation area of 32 × 32 pixels with a 50% of area overlapping. Spurious vectors produced by the cross-correlation scheme, were threshold and replaced by new values obtained from neighbour interpolation. An indication of the quality set-up was the very small number of spurious vectors obtained after the image processing, confirming that background and illumination noise sources were minimal. In previous experiments (Huera-Huarte, 2018b,a; Huera-Huarte and Gharib, 2019), we obtained the rotational motion of the foil by processing the collected images with our processing algorithms, showing very good agreement with the measurements provided by the potentiometer. An overall combined value for the uncertainty in the DPIV measurements being conservative, is estimated to be under 5%. A discussion on sources of error associated with DPIV appears in Willert and Gharib (1991) and in more detail regarding the processing techniques in Huang et al. (1997). Details of the experimental set-up are depicted schematically in Fig. 1.

3. Results and discussion

Experiments were conducted by actuating the foil with an amplitude θ_0 of 35 degrees and a frequency f of 1 Hz. For each experiment, data was recorded for 45 s, therefore over 40 flapping cycles are available in each test. The distance h from the upper edge of the foil to the free surface was varied from more than $1s$ to 0. Among all the dimensionless parameters involved in the present problem, the Reynolds number ($Re = Uc/\nu$), the Froude number ($F_r = U/\sqrt{gs}$) and the aspect ratio of the foil ($AR = s/c$), remained constant, with values around 17600, 0.17 and 1.76 respectively, because of fixed imposed kinematics and geometry. In the expressions, U is the average foil trailing edge velocity, ν is the kinematic viscosity of the fluid and g is the acceleration of gravity. The submergence depth to span ratio (h/s) is the parameter that governs the problem as it accounts for the separation between the foil and the free surface, and was systematically varied. The effect of U, AR, Re and other parameters in the performance of pitching foils has been widely studied in the past (Buchholz and Smits, 2005; Floryan et al., 2017; Huera-Huarte, 2018b; Wu et al., 2020), this is why this work is only focused in the analysis of the effects of submergence depth.

The hydrodynamic forces (F_x, F_y) and moment (M_z) seen by the foil while pitching sinusoidally with instantaneous angular velocity (Ω), are

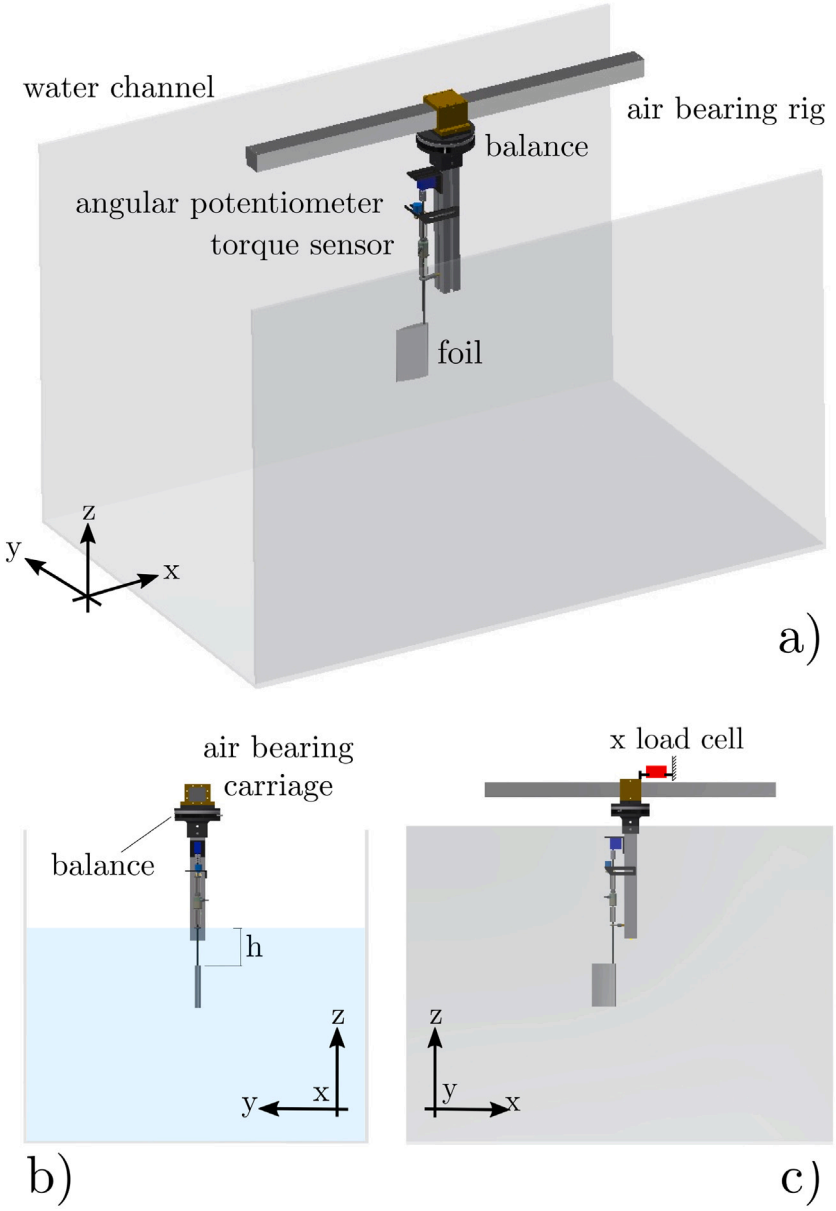

Fig. 1. Schematic views of the robotic fin used for the experiments. Cartesian origin is displaced from its actual location. Air bearing rig supporting structure not shown for the sake of clarity.

also part of the dimensionless set to study, and result of applying the following expressions,

$$C_T = \frac{F_x}{\frac{1}{2}\rho U^2 cs} \qquad C_S = \frac{F_y}{\frac{1}{2}\rho U^2 cs} \qquad C_M = \frac{M_z}{\frac{1}{2}\rho U^2 cs^2} \tag{1}$$

in which ρ is the fluid density. Mechanical power ($M_z\Omega$), efficiency and the ratio thrust to side force are defined according to the expressions below.

$$C_P = \frac{M_z\Omega}{\frac{1}{2}\rho U^3 cs} \qquad \eta = \frac{\overline{C}_T}{\overline{C}_P} \qquad \zeta = \frac{\overline{C}_T}{\widetilde{C}_S} \tag{2}$$

Thrust coefficient appears time averaged ($\overline{C}_T$) in the first column of Fig. 2, together with the standard deviation of the side force and the moment ($\widetilde{C}_S$ and $\widetilde{C}_M$) seen by the shaft, as a function of the gap distance between the foil and the free surface (h/s). In the second column of the figure the time averaged power coefficient $\overline{C}_P$ is shown as a function of distance. The inset in that plot shows the data points together with an exponential fit (dashed line) of expression $\overline{C}_P = 0.7e^{-9.7(h/s)} + 4$. The last two rows of the second column are for the efficiency (η) and the ratio thrust to side force (ζ).

The figure shows that when thrust starts to decrease, at $h/s = 0.4$, power starts to increase up to the point at which the foil is at the free surface, where it becomes maximum. Efficiency depicts a trend similar to the thrust, starting slightly under 0.2, decreasing to 0.18, reaching a minimum at 0.11 and going back to a value of 0.16 at the free surface. The same happens with the ratio of thrust to side force. The data shows clearly the non-linear effect on the propulsive characteristics of the foil, caused by the proximity to the free surface. For large separations ($h/s > 0.6$) there are practically no variations in the coefficients, but as the foil approaches the free surface there are major changes. In the case of the thrust, the variations are especially complex. There is a small first decrease of approximately 5% in the thrust coefficient, from the reference value of 0.77 to 0.73, for distances in the range $0.15 \leq h/s < 0.4$. A more important drop, with a reduction higher than a 35% in the value of thrust, takes place when the separation is less than 0.15, going to values near 0.5. When the upper edge of the foil is at the free surface, thrust level goes back to more than

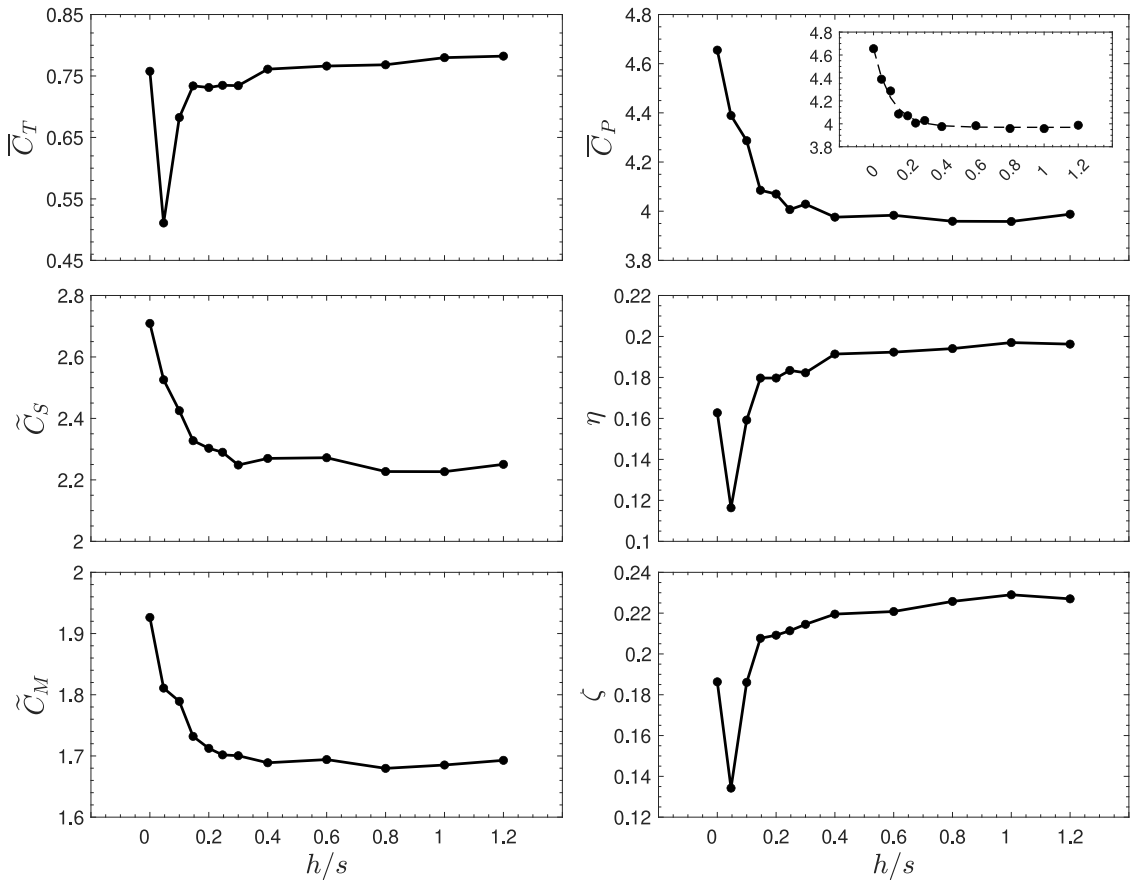

Fig. 2. Dimensionless thrust ($\overline{C}_T$), side force ($\widetilde{C}_S$), moment ($\widetilde{C}_M$), power ($\overline{C}_P$), efficiency (η) and ratio thrust to side force (ζ), as a function of the dimensionless distance to the free surface (h/s).

0.75, near the reference ones. The trends exhibited by the side force and the moment are very similar with a monotonic increase in their values as the distance to the free surface is decreased. From these two plots it appears evident that swimming by pitching an appendage perpendicularly and near to the free surface, implies a reduced thrust coefficient combined with a high absorbed power that ultimately yields a low efficiency. The loss in efficiency is approximately a 40% respect the reference values, i.e. without free surface influence. Zhu et al. (2006) showed, using numerical experiments, how as the aspect ratios of the foil were increased, the effect of the free surface was weaker. They investigated two foils, one with aspect ratio 1 and another with aspect ratio 5. In the small aspect ratio case they found reduction of thrust and propulsion efficiency with a much larger free-surface influence, with reductions in efficiency up to a 40%, in the order of the ones reported here. For the largest aspect ratio, variations were under 10%. They explained the effect as a consequence of a larger effective submergence depth as the aspect ratio was reduced. They also observed in their computations, that the surface distortion consisted of unsteady waves that propagated mostly in the transverse direction, diminishing the effect on the flapping foil wake dynamics, although the wake structures were not reported and investigated.

The monotonic increase in power observed in Fig. 2, seems intuitive if one thinks in the fact that as the free surface gets closer to the foil, part of the power will be used to generate surface deformations (Zhu et al., 2006). Conversely, the case of the thrust evolution with distance to the boundary, and the reason for the strong decay near the free-surface, seems to be much more complex and not as evident. In fact, one could easily miss this large drop in performance if the experiments would have been done by varying h/s in larger steps, as everything happens in a narrow band of separation values. This effect, has not been reported in detail previously in the available literature.

As described in Section 2, DPIV interrogations were carried out at two different planes (yz and xy) to elucidate the causes for the performance trends presented in Fig. 2. Fig. 3 shows the wake structures in a yz plane near the trailing edge of the foil, using dimensionless vorticity ($\omega_x^* = \omega_x c/U$) maps, for three cases with gap distances between the upper edge of the foil and the free surface (h/s), of 1, 0.1 and 0, in the upper (plots a to d), central (plots e to h) and lower (plots i to l) rows of the figure, respectively. The velocity vector field is also included using dark grey vectors. For each case, four phase averaged maps are shown, at phases $\theta = 0$ (first column), $\theta = \pi/4$ (second column), $\theta = \pi/2$ (third column) and $\theta = 3\pi/4$ (fourth column), i.e. for the first half of the flapping cycle, as the second one is effectively symmetric. Since the deformation of the free surface was not measured, the horizontal blue line in plots e to l, is used only for reference, to indicate the position of the free surface in the rest position, before the start of the experiment. An arrow around the shaft is used to indicate the direction of the rotation of the foil in each particular phase position.

The flow structures revealed by the vorticity maps for cases with gaps larger than $0.4s$ are all very similar, hence the case with $h/s = 1$, in the upper row, is used as the reference case depicting no influence of the free surface. This is coherent with what Fig. 2 indicates in terms of performance. In the reference case (plots a to d), when the foil reaches the maximum excursion and starts moving after changing direction, an elliptic vortex ring is shed. The yz sectional view shows a counter-rotating vortex pair that travels perpendicular to the shaft until it disappears outside the field of view. This is in fact the cross-sectional view of the vortex ring that moves not only in plane but also out-of-plane, carrying momentum in both y and x directions, with the latter being responsible for impulse and thrust (Huera-Huarte and Gharib, 2017; Huera-Huarte, 2018b). In the reference case, the flow structures are virtually symmetrical respect to the y direction at the mid span of

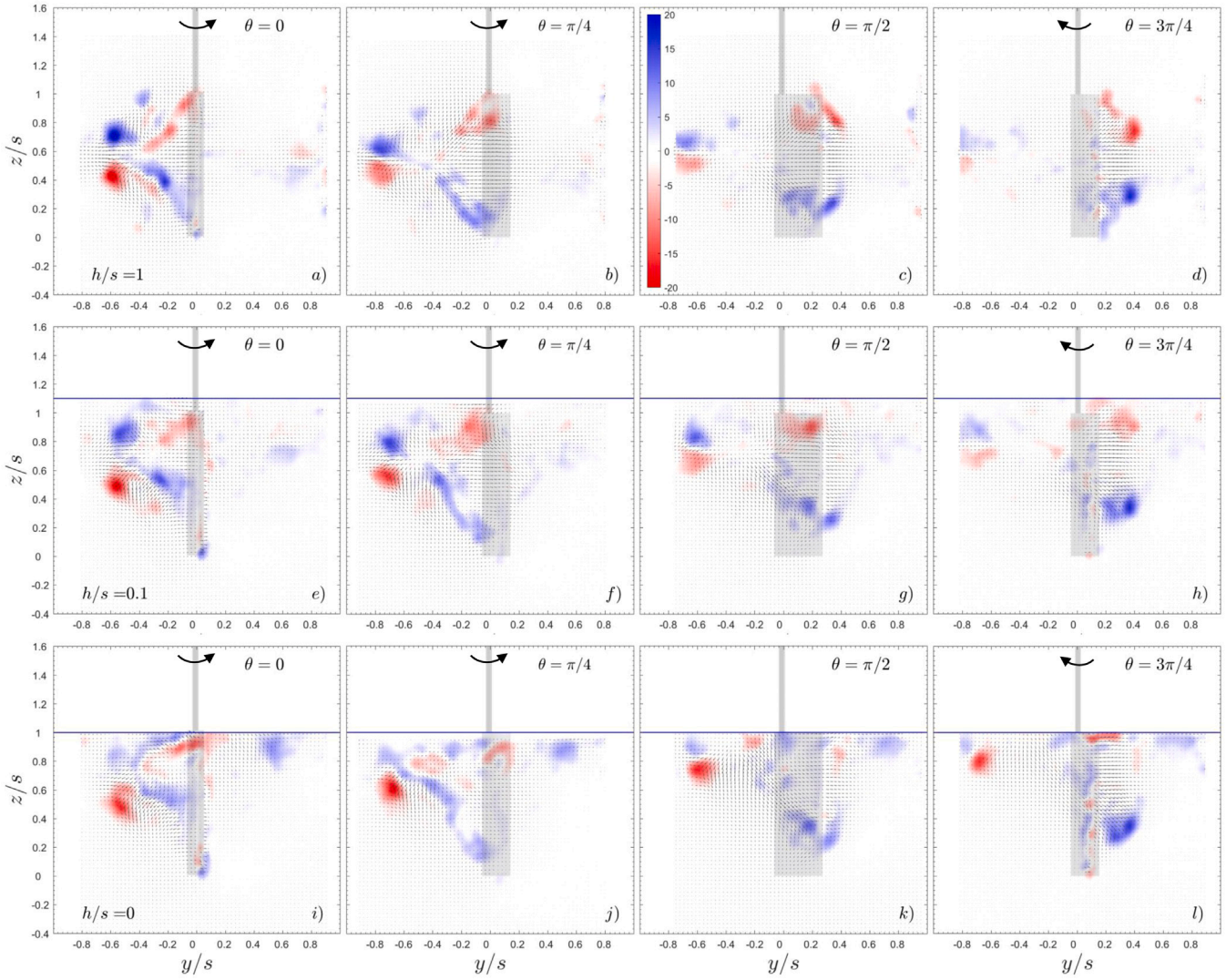

Fig. 3. Dimensionless phase averaged vorticity maps ($\omega_x^* = \omega_x c/U$), obtained at distances to the free surface (h/s) 1, 0.1 and 0 (in rows). For each case four snapshots are shown (in columns). The horizontal line in the plots is used for reference, to indicate the position of the free surface in the rest position, before the start of the experiment.

the foil. The vorticity structures generated at the upper and lower edges of the foil connect with those at the trailing edge to form the vortex ring at the other side of the foil in the next half cycle. In the yz sectional view they are seen with an inclination of approximately 45 degrees respect to the y direction.

If vorticity can be considered to be confined in a thin vortex loop, the force generated by a panel rotating in a fluid, scales with time rate of change of the circulation and the size of the vortex formed (Wu, 1981; Saffman, 1995). In other words, thrust results from the reaction to the momentum injected to the wake structures, and it is related to the time evolution of the size of the structures and the vortex strength imposed by the motion. This gives a qualitative way of explaining the forces measured by observing the wakes structures generated. A larger vortex structure, i.e. a more separated counter-rotating vortex pair in the yz cross-sectional views presented, and a larger vorticity, imply larger force. All these features are all well known from previous experiments carried out with moving surfaces of similar aspect ratios (Kim and Gharib, 2011; Flammang et al., 2011; DeVoria and Ringuette, 2012; Huera-Huarte and Gharib, 2017; Huera-Huarte, 2018a; Huera-Huarte and Gharib, 2019).

When the gap between the upper edge of the profile and the free surface is reduced, the flow structures change considerably as can be seen in the other two cases (plots e to l). The symmetry observed in the reference case is lost, as a direct consequence of the gap reduction. In the case with $h/s = 0.1$ (plots e to h), the cross-sectional view of the annular vortex, i.e. the counter-rotating vortex pair, moves towards the free surface with an inclination and the elongated structure being shed from the upper edge of the foil, has a smaller angle respect to the y direction. This new orientation of the vortex structures formed implies the generation of momentum not only in the x and y directions as in the reference case, but also in the span-wise z direction. Moreover, vortices in this case, are inclined towards the free surface and have less strength. This asymmetry is mainly caused by the increased velocities at the gap between the foil and the free surface, caused by the channelling effect at the gap, that results in unbalanced circulations producing the upward tilting of the vortex structure. This yields to a much more complex wake, the generation of free surface waves and complex interactions at the free-surface as reported by Weigand and Gharib (1995). The force measurements presented here (Fig. 2), show increased torques and therefore power needed to produce the free surface deformation, as well as a largely reduced thrust. The thrust reduction is related to the appearance of the span-wise momentum generated, in detriment of that generated in the y and x directions, as well as to the weakening of the vorticity near the free surface. The objectives of the present work is the analysis of the influence of the free surface in the overall propulsive performance of the pitching

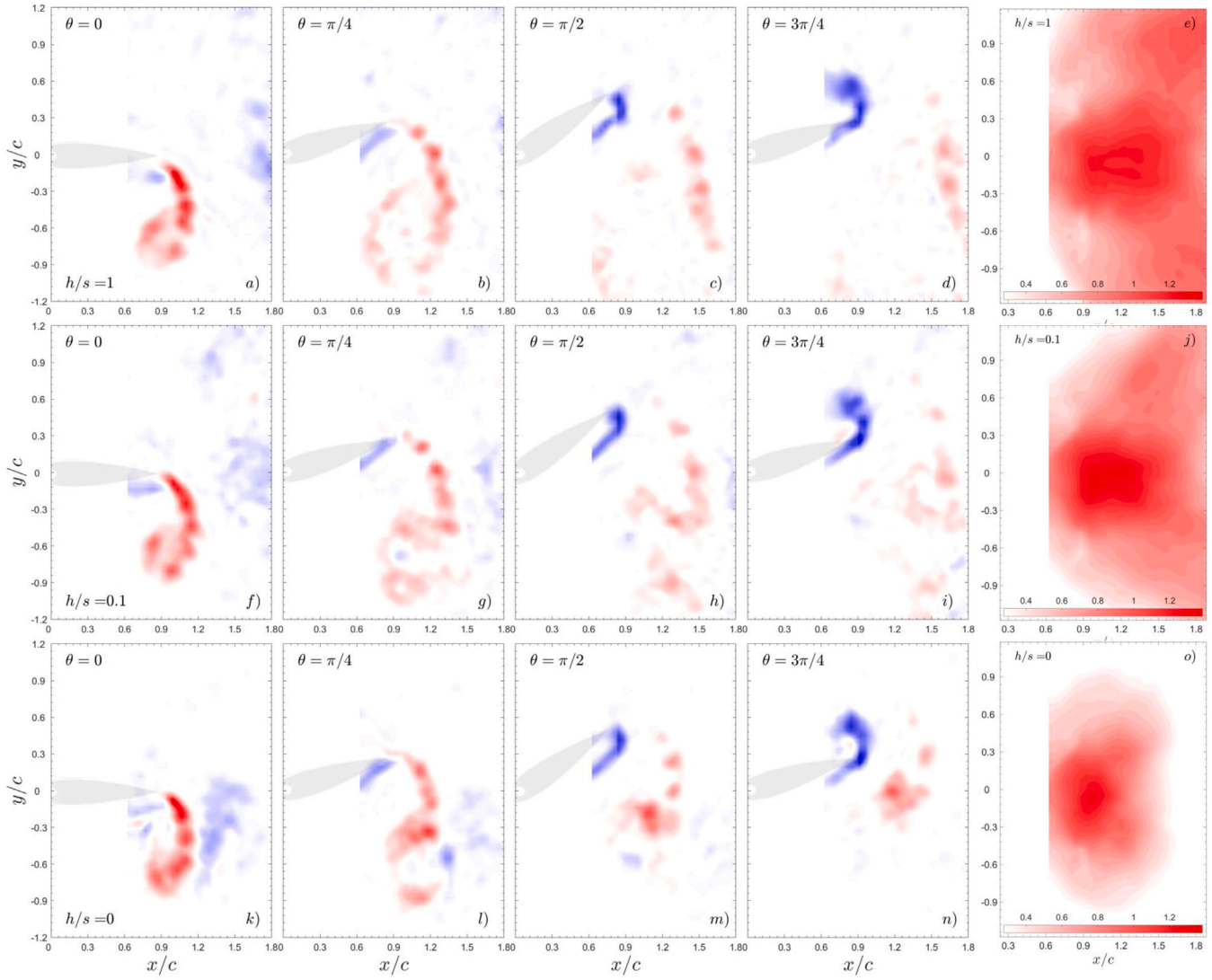

Fig. 4. Dimensionless phase averaged vorticity maps ($\omega_z^* = \omega_z c/U$), obtained at distances to the free surface (h/s) 1, 0.1 and 0 (in rows). The last column shows the magnitude of the velocity non-dimensionalized with U. For each case four snapshots are shown (in the first four columns).

foil and not the analysis of the intricate details of vortex interaction and evolution near the free surface. That particular topic was studied by Bernal et al. (1989), and Bernal and Kwon (1989), with pioneering studies on the interaction between vortex rings evolving parallel and perpendicular to the free surface. Following these studies, Weigand and Gharib (1995) and Gharib and Weigand (1996) looked into the process of vortex connections and disconnections at the free surface, of a vortex ring travelling with different inclinations and depths respect the free surface.

In the last row of Fig. 3, in plots i to l, there is no separation between the free surface and the foil ($h/s = 0$). The upper vortex, i.e. the upper part of the cross-sectional view of the ring, practically disappears and the lower one travels rapidly towards the free surface, indicating that the vortex ring is open and connects in the upper part to the free surface. This can be easily seen in plot 3l, where only the lower vortex can be identified. Only part of the ring is generated because of the connection with the free surface that leaves it open (Weigand and Gharib, 1995). The elongated structure being shed from the lower edge has moved towards the mid-span and it is tilted. The size of the half annular structure is larger than in the other two cases, in fact, if the vortex was not cut at the free surface, it would have approximately double the size of the one in the reference case. Here, the free surface acts as the symmetry plane instead of being at mid span of the foil. From the propulsive performance point of view, the larger size and the strength, that seems not to be largely altered respect to the reference case, should result in larger force coefficients, and this is what Fig. 2 showed, with a thrust level that stays at values similar to the ones observed without free surface effects.

The lost of symmetry induced by the proximity to the free surface and the consequent loss of performance of the flapping system, does not appear evident in the xy DPIV interrogations shown in Fig. 4, obtained by measuring at the mid-span of the foil. In the first four columns of the figure from the left, vorticity appears in dimensionless form ($\omega_z^* = \omega_z c/U$), again for the same phase averaged positions of the foil. Plots a to d in Fig. 4 show the xy view of the reference case. The vortices that appear there, are cross-sectional views of the part of the ring that goes between the cross-sectional view of the vortex pair seen in plane yz from Fig. 3, confirming again the annular structure in the wake. The formation of a clockwise rotating tip vortex can be seen until the foil reaches the maximum excursion, point at which the chord-wise flow in the foil starts to generate counter-clockwise circulation that yields a bound vortex that cuts the previous structure that continues moving in the x direction towards the end of the field of view. This vortex pair is the cross-sectional view of the same vortex ring described previously, whereas here the inclination respect to the xz plane can be seen in this view. The last column of the figure (plots e, j and o) is for the

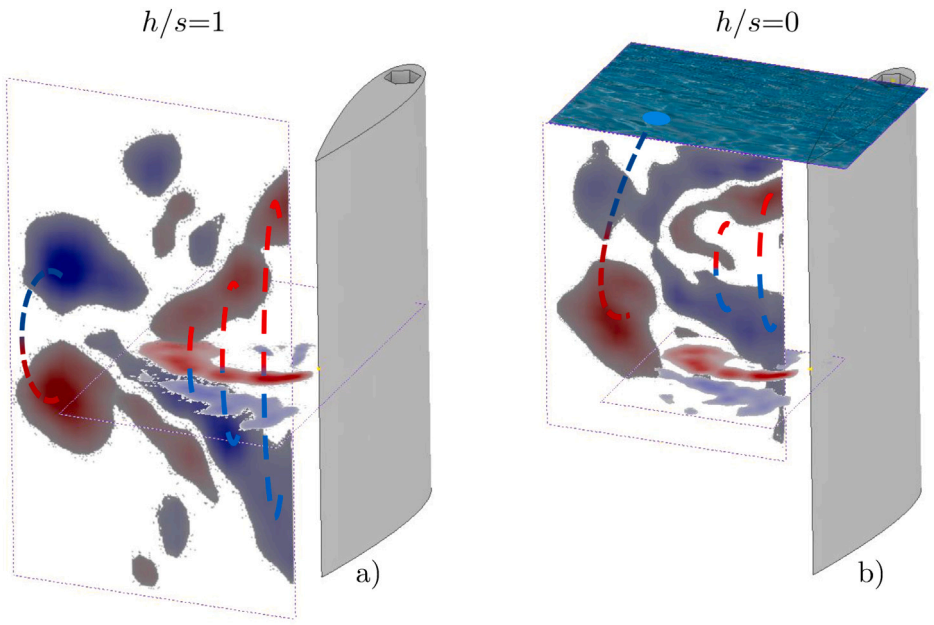

Fig. 5. Three-dimensional schematic reconstruction of the wake based on the planar phase averaged DPIV yz and xy interrogations performed, for the reference case $h/s = 1$ and for the case with the upper edge of the foil at the free surface $h/s = 0$. Both views are for the position of the foil inside the cycle, with phase $\theta = 0$.

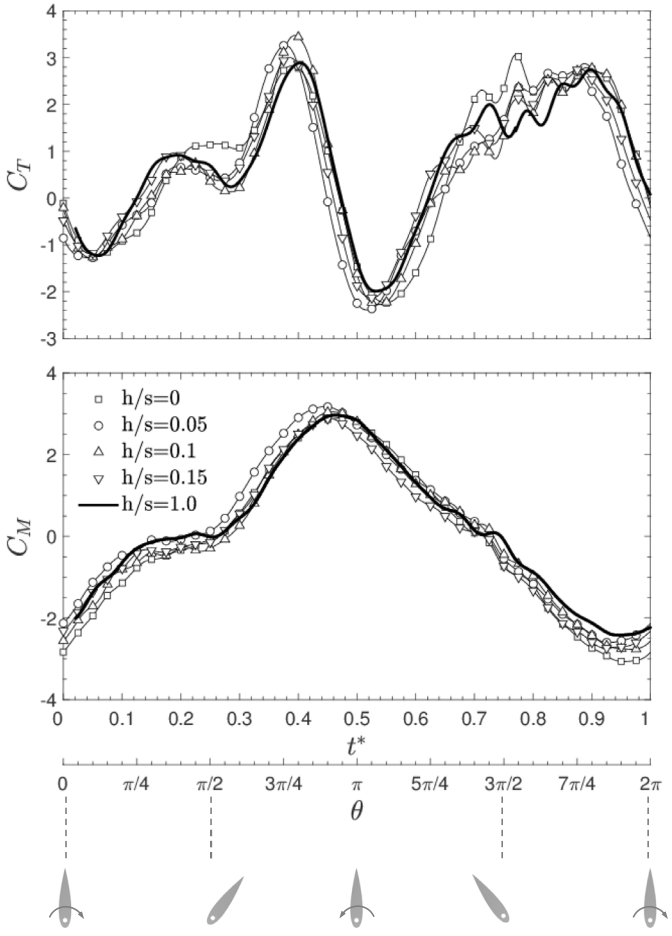

Fig. 6. Cycle averaged time series of the dimensionless coefficients of thrust (C_T) and moment (C_M), for the reference case (solid line) and for other representative cases shown in Fig. 2. Time is shown in dimensionless form ($t^* = ft$).

magnitude of the velocity non-dimensionalized with U. The plot shows only velocities that are equal or larger than 30% of the tip velocity U, for the sake of clarity. As in Fig. 3, each row in the figure is for a different h/s, from 1 in the upper row to 0 in the lower one as in the previous figure. From the last column it is clear that the region covered by large velocities becomes smaller and closer to the foil as the free surface is near to the upper edge. Moreover, the vorticity maps show how the tip vortex does not dissipate as fast as in the other two cases and remains closer to the trailing edge of the foil when near the free surface. This view evidences the fact that in the free surface case, the symmetry plane of the vortex formation is not at the mid span as in the reference case, but at the free surface, therefore the xy cross-sectional view shows the vortices closer to the trailing edge.

A three-dimensional schematic reconstruction of the wake based on the planar DPIV yz and xy interrogations performed appears in Fig. 5, for the reference case $h/s = 1$ (left plot 5*a*) and for the case with the upper edge of the foil at the free surface $h/s = 0$ (right plot 5*b*). They show the phase averaged dimensionless vorticity planes for phases $\theta = 0$, that appear in Fig. 4a and i, respectively. The views are qualitative only, with the purpose to provide an easier interpretation of the planar measurements carried out, and to support the explanations given above. Dashed lines are used to indicate the approximate path of the vortex cores and circulation regions. The case with $h/s = 0.1$, that appears in Figs. 3 and 4 has not been included here as the only qualitative difference to the reference case shown in 5a is the fact that the counter-rotating pair that form the ring indicated in the figure is tilted and moves with an inclination towards the free surface, as commented before.

To further discuss the results, Fig. 6 illustrates the times series of thrust and moment coefficients for several cases presented in Fig. 2, with $h/s = 0$, 0.05, 0.1, 0.15 and 1. The data appears cycle averaged, resulting from more than 40 cycles, as a function of the dimensionless time $t^* = ft$ or the position of the foil θ. The solid line depicts the reference case without free surface effects. In the lower part of the figure an schematic view of the foil is shown at each position inside the cycle, for reference. When the foil moves from one side of the cycle ($\theta = \pi/2$) to the other ($\theta = 3\pi/2$), the strong circulation at the trailing edge generates a strong vortex at the tip (see plots a, f and k from Fig. 4 and the dashed lines near the trailing edge of the three-dimensional representation of Fig. 5a) that makes the thrust and

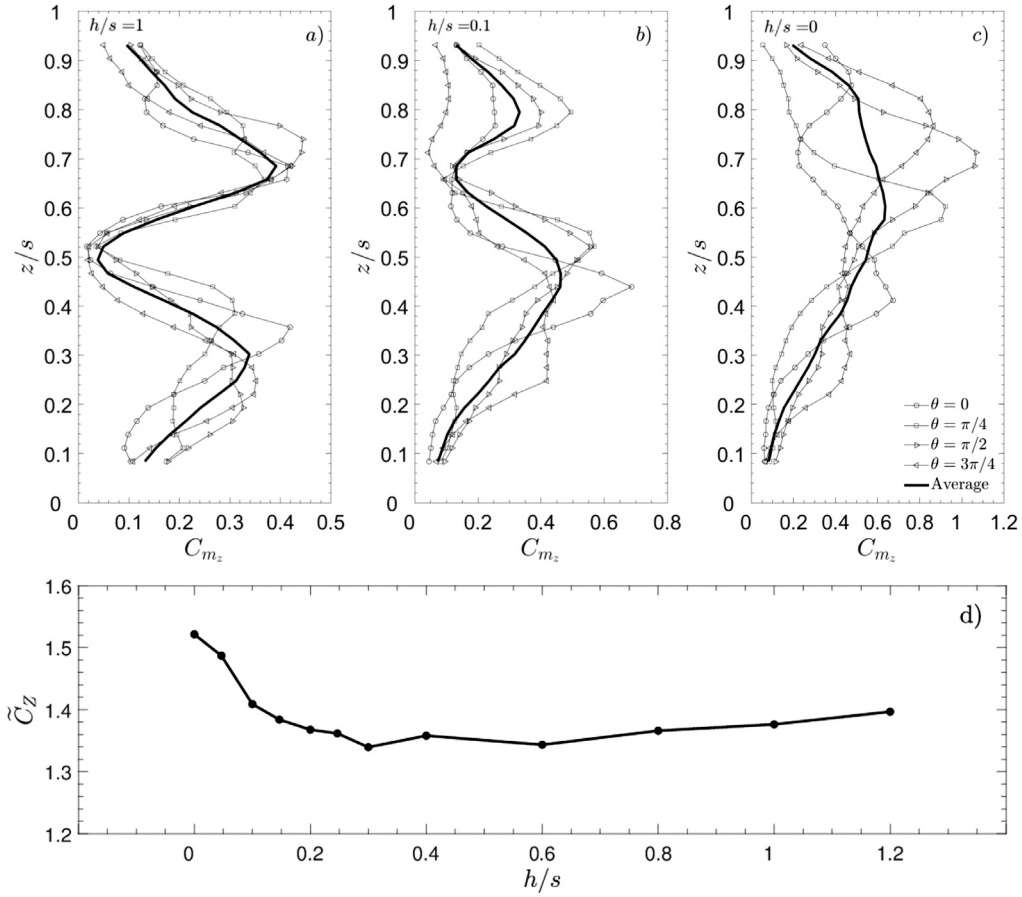

Fig. 7. Momentum flux coefficients in the span-wise direction (C_{m_z}) obtained at distances to the free surface (h/s) 1, 0.1 and 0 (plots *a*, *b* and *c*, respectively). Root mean square value of the dimensionless vertical force coefficient ($\widetilde{C_Z}$) for the same cases.

the moment coefficients increase up to their maximum values, just before reaching the central position at $t^* = 0.5$, and then starts to decrease to their minimum value of thrust and zero moment, just after the central position. As it continues to the other side of the flapping cycle it starts to grow again to and intermediate peak produced by the shedding of the bound vorticity (see plots *d*, *i* and *n*) from Fig. 4. The latter results from the flow travelling chord-wise to the trailing edge. Just after this event the foil starts to move again in the other direction building up circulation at the tip to reach the maximum thrust and moment just before the central position, as in the previous half cycle. The detailed description of the vortex formation process in pitching foils has been studied by the author in the past observing the same general features (Huera-Huarte and Gharib, 2017; Huera-Huarte, 2018b; Huera-Huarte and Gharib, 2019). Here, the time series clearly show that for the case without free surface effects, the average thrust is larger than in the rest of cases, as seen in Fig. 2, as most of the points in the plots (with the exception of the peaks) appear over the rest of cases. This is more evident with $h/s = 0.05$ where the lowest thrust was recorded. The moment shows clearly how absolute values for the reference case are smaller that those of the other cases, during all the cycle.

All these modifications observed in the wake structure as a function of the distance to the free surface, explain the propulsive performance reported in Fig. 2. They govern the way momentum is injected to the wake, which depends on parameters such as the imposed kinematics and the geometry of the foil (Shinde and Arakeri, 2013; Park et al., 2016; Heathcote et al., 2004; Huera-Huarte and Gharib, 2017; Huera-Huarte, 2018b; Shinde and Arakeri, 2018). Huera-Huarte and Gharib (2019) showed that thrust and performance can be actively altered by changing the way momentum is injected to the wake, by changing the geometry of the wake, using a foil with an active trailing edge. To further study the effect of the free surface, in Fig. 7, the vertical force coefficient (C_Z) and the momentum flux coefficients (C_{m_z}) along the z direction for the cases in Fig. 3, are presented. These are computed based on equations,

$$C_{m_z} = \frac{2}{U^2 l_y}\int_{y_1}^{y_2} w^2 dy \qquad C_Z = \frac{F_z}{\frac{1}{2}\rho U^2 cs} \tag{3}$$

where w is the velocity component in the z direction, and l_y is the length in the y direction in which the finite integrals are evaluated. The vertical force coefficient is presented in the lower row of the figure (plot d), using its root mean square value ($\widetilde{C_Z}$), as it was measured with the 6-axis balance. The plots in the upper row of the figure are for cases with $h/s = 1$, 0.1 and 0 from left to right columns. Symbols are used for each phase inside the cycle as in Figs. 3, and the solid line is the time averaged momentum flux over the whole cycle.

In the upper left corner (plot a), the C_{m_z} in the reference case shows a momentum flux across y as a function of z, that is symmetric respect the mid span, resulting from span-wise flow velocities with opposite sign at each side of the symmetry plane. The reaction to the momentum flux at the upper half of the foil must balance that at the lower half, and it is nearly zero at the mid-span. This region of the foil where the momentum flux is the smallest, moves towards the free surface as the gap between the upper edge of the foil and the free surface is reduced, as can be seen in plot b, for the case with $h/s = 0.1$. This fact indicates again the symmetry breaking in the wake, as shown with the velocity and vorticity maps of Fig. 3. When the foil is near the free surface with $h/s = 0.1$, the unbalanced span-wise momentum flux distribution suggests a non-zero net span-wise force, not existing or minimal in the reference case. The lower plot, with the vertical force coefficient,

confirms these forces, with values that are larger when near the free surface as pointed out by the DPIV analysis and the momentum fluxes reported, explaining the thrust performance trend observed in Fig. 2. The vertical force coefficient is not constant in the range 1.35 to 1.4 for h/s larger than 0.4, but it clearly grows up to 1.55 when the free surface is near. Under this situation the power that the foil needs to produce the kinematics imposed in the experiments, is not only used to generate thrust in the x direction as in the reference case, but also to generate span-wise thrust in the z direction. Moreover, extra torque is used to deform the free surface, especially in the case with the foil at the free surface, although we have not measured or quantified this effect in the present experiments. Plot c, for $h/s = 0$, shows that the free surface acts as the symmetry plane instead of the mid-span of the foil as in the reference case as suggested by the DPIV results presented previously.

4. Conclusions

Experiments conducted with a symmetric profile pitching sinusoidally, with its shaft perpendicular to the free surface, at different separation distances from it, have been conducted. The robotic system and the measurements obtained show the effect of the proximity to the free surface on the propulsive performance of the system.

The experiments reveal a highly non-linear relationship between the performance and the separation to the free surface. When the system actuates near the free surface, at a separation around 5 to 10% of its span, it suffers a dramatic decay in thrust (approximately 30%) and an increased power for given fixed imposed kinematics, implying a low efficiency, showing a drop of around 40%. The analysis of the fluid loading and the flow field around the system indicates that the free surface induces a symmetry breaking in the overall wake structure formation, resulting in span-wise flow, and in momentum redirection. If the separation is zero, with the upper edge of the profile moving at the free surface, thrust is mostly recovered but power is considerably larger than in the reference case, yielding again to a diminished efficiency. The free surface in this case, acts as the symmetry plane instead of the mid span of the foil.

Declaration of competing interest

The authors declare that they have no known competing financial interests or personal relationships that could have appeared to influence the work reported in this paper.

Data availability

Data will be made available on request.

Acknowledgements

This research was funded by the Spanish Agencia Estatal de Investigación, Spain (AEI) grant number PGC2018-097766-B-I00 and AGAUR, Spain grant 2017-SGR1263.

References

Barannyk, O., Buckham, B.J., Oshkai, P., 2012. On performance of an oscillating plate underwater propulsion system with variable chordwise flexibility at different depths of submergence. J. Fluids Struct. 28, 152–166. http://dx.doi.org/10.1016/j.jfluidstructs.2011.10.005.

Bernal, L.P., Hirsa, A., Kwon, J.T., Willmarth, W.W., 1989. On the interaction of vortex rings and pairs with a free surface for varying amounts of surface active agent. Phys. Fluids A 1 (12), 2001–2004, URL http://link.aip.org/link/PFADEB/v1/i12/p2001/s1{&}Agg=doi.

Bernal, L.P., Kwon, J.T., 1989. Vortex ring dynamics at a free surface. Phys. Fluids A 1 (3), 449–450.

Buchholz, J.H.J., Smits, A.J., 2005. On the evolution of the wake structure produced by a low-aspect-ratio pitching panel. J. Fluid Mech. 546 (-1), 433.

Buren, T.V., Floryan, D., Smits, A.J., 2020. Bioinspired underwater propulsors. In: Soboyejo, W., Daniel, L. (Eds.), Bioinspired Structures and Design. Cambridge University Press, pp. 113–139.

Cleaver, D.J., Calderon, D.E., Wang, Z., Gursul, I., 2013. Periodically plunging foil near a free surface. Exp. Fluids 54 (3), 1491.

Colgate, J.E., Lynch, K.M., 2004. Mechanics and control of swimming: A review. IEEE J. Ocean. Eng. 29 (3), 660–673.

DeVoria, A.C., Ringuette, M.J., 2012. Vortex formation and saturation for low-aspect-ratio rotating flat-plate fins. Exp. Fluids 52 (2), 441–462.

Fernández-Prats, R., Raspa, V., Thiria, B., Huera-Huarte, F., Godoy-Diana, R., 2015. Large-amplitude undulatory swimming near a wall. Bioinspir. Biomim. 10 (1), 16003. http://dx.doi.org/10.1088/1748-3190/10/1/016003.

Flammang, B.E., Lauder, G.V., Troolin, D.R., Strand, T.E., 2011. Volumetric imaging of fish locomotion. Biol. Lett. 7 (5), 695–698.

Floryan, D., Buren, T.V., Rowley, C.W., Smits, A.J., 2017. Scaling the propulsive performance of heaving and pitching foils. J. Fluid Mech. 822, 386–397.

Gharib, M., Weigand, A., 1996. Experimental studies of vortex disconnection and connection at a free surface. J. Fluid Mech. 321, 59–86.

Heathcote, S., Martin, D., Gursul, I., 2004. Flexible flapping airfoil propulsion at zero freestream velocity. AIAA J. 42 (11), 2196–2204.

Huang, H., Dabiri, D., Gharib, M., 1997. On errors of digital particle image velocimetry. Meas. Sci. Technol. 8 (12), 1427. http://dx.doi.org/10.1088/0957-0233/8/12/007.

Huera-Huarte, F., 2018a. Propulsive performance of a pair of pitching foils in staggered configurations. J. Fluids Struct. 81.

Huera-Huarte, F.J., 2018b. On the Impulse Produced by Chordwise Flexible Pitching Foils in a Quiescent Fluid. Trans. ASME, J. Fluids Eng. 140 (4), 1–10.

Huera-Huarte, F.J., Gharib, M., 2017. On the effects of tip deflection in flapping propulsion. J. Fluids Struct. 71, 210–217. http://dx.doi.org/10.1016/j.jfluidstructs.2017.04.003.

Huera-Huarte, F., Gharib, M., 2019. Role of the near-tip region of a fin in fish propulsion. Phys. Rev. Fluids 4 (6).

Katz, J., 2006. Aerodynamics of race cars. Annu. Rev. Fluid Mech. 38 (1), 27–63, URL https://www.annualreviews.org/doi/10.1146/annurev.fluid.38.050304.092016.

Katz, J., Plotkin, A., 2001. Low-Speed Aerodynamics. vol. 13, Cambridge University Press.

Kim, D., Gharib, M., 2011. Characteristics of vortex formation and thrust performance in drag-based paddling propulsion. J. Exp. Biol. 214 (3), 2283–2291.

Lighthill, M.J., 1960. Note on the swimming of slender fish. J. Fluid Mech. 9 (2), 305.

Lighthill, M.J., 1969. Hydromechanics of aquatic animal propulsion. Annu. Rev. Fluid Mech. 1 (1), 413–446, URL https://www.annualreviews.org/doi/10.1146/annurev.fl.01.010169.002213.

Lighthill, M.J., 1970. Aquatic animal propulsion of high hydromechanical efficiency. J. Fluid Mech. 44 (02), 265.

Lighthill, M.J., 1971. Large-Amplitude Elongated-Body Theory of Fish Locomotion. Proc. R. Soc. B: Biol. Sci. 179 (1055), 125–138.

Park, H., Park, Y.J., Lee, B., Cho, K.J., Choi, H., 2016. Vortical structures around a flexible oscillating panel for maximum thrust in a quiescent fluid. J. Fluids Struct. 67 (April), 241–260.

Quinn, D.B., Lauder, G.V., Smits, A.J., 2014a. Flexible propulsors in ground effect. Bioinspir. Biomim. 9 (3), 036008.

Quinn, D.B., Moored, K.W., Dewey, P.a., Smits, a.J., 2014b. Unsteady propulsion near a solid boundary. J. Fluid Mech. 742, 152–170.

Saffman, P.G., 1995. Vortex Dynamics. Cambridge University Press.

Sfakiotakis, M., Lane, D., Davies, J., 1999. Review of fish swimming modes for aquatic locomotion. IEEE J. Ocean. Eng. 24 (2), 237–252, URL http://ieeexplore.ieee.org/document/757275/.

Shinde, S.Y., Arakeri, J.H., 2013. Jet meandering by a foil pitching in quiescent fluid. Phys. Fluids 25 (4).

Shinde, S.Y., Arakeri, J.H., 2018. Physics of unsteady thrust and flow generation by a flexible surface flapping in the absence of a free stream. Proc. R. Soc. A 474 (2218).

Smits, A.J., 2019. Undulatory and oscillatory swimming. J. Fluid Mech. 1–70.

Staufenbiel, R.W., Schlichting, U.J., 1988. Stability of airplanes in ground effect. J. Aircr. 25 (4), 289–294.

Thums, M., Meekan, M., Stevens, J., Wilson, S., Polovina, J., 2013. Evidence for behavioural thermoregulation by the world's largest fish. J. R. Soc. Interface 10 (78).

Triantafyllou, M.S., Hover, F.S., Techet, A.H., Yue, D.K.P., 2005. Review of hydrodynamic scaling laws in aquatic locomotion and fishlike swimming. Appl. Mech. Rev. 58 (July), 226–236.

Triantafyllou, M.S., Triantafyllou, G.S., Gopalkrishnan, R., 1991. Wake mechanics for thrust generation in oscillating foils. Phys. Fluids A 3 (12), 2835.

Triantafyllou, G.S., Triantafyllou, M.S., Grosenbaugh, M.A., 1993. Optimal Thrust development in Oscillating foils with application to fish propulsion. J. Fluids Struct. 7 (2), 205–224.

Triantafyllou, M.S., Triantafyllou, G.S., Yue, D.K.P., 2000. Hydrodynamics of Fish-like Swimming. Annu. Rev. Fluid Mech. 32 (1), 33–53, URL https://www.annualreviews.org/doi/10.1146/annurev.fluid.32.1.33.

Weigand, A., Gharib, M., 1995. Turbulent vortex ring/free surface interaction. Trans. ASME, J. Fluids Eng. 117 (3), 374–381.

Willert, C.E., Gharib, M., 1991. Digital particle image velocimetry. Exp. Fluids 10 (4), 181–193.
Wu, J.C., 1981. Theory for aerodynamic force and moment in viscous flows. AIAA J. 4 (19), 432–441.
Wu, T.Y., 2011. Fish Swimming and Bird/Insect Flight. Annu. Rev. Fluid Mech. 43 (1), 25–58, URL http://www.annualreviews.org/doi/abs/10.1146/annurev-fluid-122109-160648.
Wu, X., Zhang, X., Tian, X., Li, X., Lu, W., 2020. A review on fluid dynamics of flapping foils. Ocean Eng. 195, 106712. http://dx.doi.org/10.1016/j.oceaneng.2019.106712.
Zhu, Q., Liu, Y., Yue, D.K., 2006. Dynamics of a Three-Dimensional Oscillating Foil Near the Free Surface. AIAA J. 44 (12), 2997–3009.